

Search for sub-mm, mm and radio continuum emission from extremely red objects

Niruj R. Mohan^{1,2}, A. Cimatti³, H. J. A. Röttgering⁴, P. Andreani^{5,6}, P. Severgnini⁷,
R. P. J. Tilanus⁸, C. L. Carilli⁹, and S. A. Stanford¹⁰

¹ Raman Research Institute, C.V. Raman Avenue, Sadashivanagar, Bangalore 560080, India

² Joint Astronomy Program, Department of Physics, Indian Institute of Science, Bangalore 560012, India

³ Osservatorio Astrofisico di Arcetri, Largo Fermi 5, 50125 Firenze, Italy

⁴ Sterrewacht Leiden, Sterrewacht, Postbus 9513, Leiden 2300 RA, The Netherlands

⁵ Max-Planck Institut für Extraterrestrische Physik, Postfach 1312, 85741 Garching bei Muenchen, Germany

⁶ Osservatorio Astronomico di Padova, vicolo dell' Osservatorio 5, 35122 Padova, Italy

⁷ Dip. Astronomia, Università di Firenze, Largo E. Fermi 5, 50125 Firenze, Italy

⁸ Joint Astronomy Centre, 660 N. Aohoku Place, Hilo, HI 96720, USA

⁹ NRAO, PO Box 0, Socorro NM, 87801, USA

¹⁰ Institute of Geophysics and Planetary Physics, Lawrence Livermore National Laboratory, L-413, PO Box 808, Livermore, CA 94550, USA

Received 24 September 2001 / Accepted 5 December 2001

Abstract. We present the results of sub-mm, mm (850 μm , 450 μm and 1250 μm) and radio (1.4 and 4.8 GHz) continuum observations of a sample of 27 K -selected Extremely Red Objects, or EROs, (14 of which form a complete sample with $K < 20$ and $I - K > 5$) aimed at detecting dusty starbursts, deriving the fraction of UltraLuminous Infrared Galaxies (ULIGs) in ERO samples, and constraining their redshifts using the radio-FIR correlation. One ERO was tentatively detected at 1250 μm and two were detected at 1.4 GHz, one of which has a less secure identification as an ERO counterpart. Limits on their redshifts and their star forming properties are derived and discussed. We stacked the observations of the undetected objects at 850 μm , 1250 μm and 4.8 GHz in order to search for possible statistical emission from the ERO population as a whole, but no significant detections were derived either for the whole sample or as a function of the average NIR colours. These results strongly suggest that the dominant population of EROs with $K < 20$ is not comprised of ULIGs like HR 10, but is probably made of radio-quiet ellipticals and weaker starburst galaxies with $L < 10^{12} L_{\odot}$ and $SFR < \text{few hundred } M_{\odot} \text{ yr}^{-1}$.

Key words. galaxies: elliptical and lenticular, cD – galaxies: general – galaxies: high-redshift – infrared: galaxies – radio continuum: galaxies – submillimeter

1. Introduction

The existence of a population of extragalactic objects with extremely red infrared-optical colours has been known for a number of years (for a recent review, see Cimatti 2000). These objects were initially discovered mainly in near-infrared surveys of blind fields and quasar fields and are very faint or invisible in the optical bands (Elston et al. 1988; McCarthy et al. 1992; Hu & Ridgway 1994). These extremely red objects (EROs) are defined as those which have $R - K$ colours ≥ 5 and these tend to have K magnitudes fainter than ~ 18 . Since the time of their discovery, the nature of this population has remained a puzzle. Based on their NIR and optical photometric data, two

broad classes of models are consistent with the observed red colours: (a) high redshift starbursts, red because of severe dust extinction. From the required extinction and simple dust models, these galaxies could be normal starburst galaxies or even high- z counterparts of local Ultra Luminous Infrared Galaxies (ULIGs) and (b) old passively evolving ellipticals at redshifts greater than about one. The red colours of the EROs would then be explainable by a large K -correction and an absence of ongoing star formation. If the EROs belong to the former class, then they would be dominant sites of star formation and would be important in determining the star formation history of the universe (Cimatti et al. 1998a). On the other hand, if they belong to the latter class, then the volume density of these objects as a function of redshift would pose strong constraints on the models for the formation of

Send offprint requests to: N. R. Mohan,
e-mail: niruj@rri.res.in

elliptical galaxies, which range from monolithic collapse to dark matter dominated hierarchical structure formation scenarios (Daddi et al. 2000b and references therein).

Over the last few years, it has been possible to study in detail a handful of EROs which are bright enough to yield reliable spectra and have multi-wavelength continuum data. These studies were able to determine the nature of these EROs and there are now examples known for both starbursts (Cimatti et al. 1998a; Cimatti et al. 1999; Smail et al. 1999a; Smail et al. 1999b; Gear et al. 2001) as well as for old ellipticals (Spinrad et al. 1997; Cimatti et al. 1999; Soifer et al. 1999; Liu et al. 2000) among the ERO population. Studies indicate though, that not more than $\sim 30\%$ of EROs are starbursts (see Sect. 5 for details). Recently, independent wide-field surveys for EROs have been conducted (Daddi et al. 2000a; McCarthy et al. 2000; Thompson et al. 1999) which have shown that these objects are strongly clustered in the sky (see also Chapman et al. 2000; Yan et al. 2000). The surface density of these EROs after correcting for clustering, assuming that these are passively evolving ellipticals, has been shown to be consistent with pure luminosity evolution with a formation redshift greater than 2.5 (Daddi et al. 2000b).

HR 10 is one of the reddest EROs and is quite bright in the NIR ($I - K = 6$, $K = 18.42$, Graham & Dey 1996). Cimatti et al. (1998a) detected $850 \mu\text{m}$ and $1250 \mu\text{m}$ emission from this object (see also Dey et al. 1999). They derived a star formation rate of several hundred $M_{\odot} \text{ yr}^{-1}$ and an FIR luminosity in excess of $10^{12} L_{\odot}$, thus showing that HR 10 is an ULIG at its redshift of 1.44 (Graham & Dey 1996). At the time of the observations presented in this paper, HR 10 was the only ERO with detected submm emission and also the only ERO with a known redshift. Hence it was thought possible that a majority of EROs would be similar to HR 10 and would have observable submm and mm emission (Cimatti et al. 1998b; Andreani et al. 1999). Therefore we began a search for mm and sub-mm continuum emission from other EROs with an aim to detect extreme starburst galaxies. Further, in order to constrain the redshifts of these objects and also to understand their nature, we also decided to search for radio continuum emission from these EROs.

The radio and the FIR luminosities of nearby galaxies ($z < 0.4$) which are dominated by star formation are known to be highly correlated (see Condon 1992 and references therein), whereas E and S0 galaxies are known to be more radio bright than a star-forming galaxy of similar FIR luminosity (Walsh et al. 1989). The radio (mainly synchrotron and some amount of free-free) emission and the FIR (due to dust) emission have different spectral indices. Hence, assuming the local radio-FIR correlation holds at high redshift, the observed ratio of radio to FIR emission strengths can be used to determine the redshift of a star-forming galaxy (the redshift determination method and the associated error estimation are developed in Carilli & Yun 1999, 2000; Blain 1999).

So, if on the one hand, the ERO population consists primarily of starbursts, this method could be used to

determine the nature of EROs and also to constrain the redshifts of these objects. If, on the other hand, the EROs are ellipticals, their IR colours would be used to constrain their properties. Since most EROs are too faint to obtain redshifts even with 10 m-class telescopes or even to obtain accurate photometry over the entire optical-IR range, such complementary diagnostics become important in understanding these objects.

We first describe the ERO sample, the observations and their results in Sects. 2 and 3. In Sect. 4, we derive statistical properties of the sample and estimate the fraction of starbursts and ellipticals with radio emission in Sect. 5. Those EROs with radio or mm detections are discussed in detail and their properties are derived in Sect. 6. The cosmology adopted in this paper is a flat universe with $H_0 = 70 \text{ km s}^{-1} \text{ Mpc}^{-1}$ and all results are calculated for both $\Omega_{\Lambda} = 0.7$ and $\Omega_{\Lambda} = 0.0$. The spectral index is assumed to be -0.7 throughout this paper for calculating the K -correction for the radio emission.

2. Sample and observational details

A sample of 27 EROs was selected from the literature and also from other samples being studied by the authors. These objects were identified from a variety of observations: deep NIR surveys of random fields, galaxy cluster fields and quasar fields (see references in Table 1).

A $R - K$ or an $I - K$ lower cut-off of 5 was used to select these EROs. Given the heterogenous nature of the fields from which these objects were taken, the sample as a whole is not complete or uniform. However, a subset of the objects observed, the EES sub-sample (Elston et al. 2001) does form a *complete* sample of 14 EROs, selected such that $K < 20$ and $I - K > 5$, and are listed separately in Table 1. Hereafter, the term ERO will imply all 27 objects listed in the table and the EES sample will include only the 14 objects forming a complete sample. The average $R - K$ and $I - K$ colours of the EES sample and the rest of the EROs are statistically indistinguishable. A sub-sample of the EROs selected was observed at $1250 \mu\text{m}$ using the IRAM 30 m telescope (15 objects) and at $850 \mu\text{m}$ (21 objects) and $450 \mu\text{m}$ (5 objects) using the SCUBA at the JCMT. Some of these objects have also been observed either at 4.8 GHz or at 1.4 GHz (11 and 7 objects respectively) using the VLA. Due to various telescope scheduling constraints, the same objects could not be observed at all wavebands.

2.1. NIR observations of the EES complete sub-sample

Elston et al. (2001) have completed a *BRIzJK* field survey (hereafter, EES survey) covering $\sim 100 \text{ arcmin}^2$ over four areas of the sky at high galactic latitudes, down to $K \sim 21.5$. These observations were carried out at the 4 m telescope of the Kitt Peak National Observatory. Optical imaging was obtained with the PFCCD/T2KB, which gives $0.48''$ pixels over a $16'$ field. The IR imaging was obtained with IRIM, in which a NICMOS3 HgCdTe

Table 1. NIR and optical broadband magnitudes of EROs.

| Galaxy | RA (J2000.0) | Dec (J2000.0) | K^a (mag) | $J - K$ (mag) | $I - K$ (mag) | $R - K$ (mag) | Ref |
|-----------------------------------|---|------------------|----------------|------------------|------------------|------------------|-----|
| EES Sample | | | | | | | |
| EES-Lynx 1 | 08 ^h 48 ^m 30 ^s .82 | +44°52′51″ | 19.8 | 2.4 | 5.4 | >6.2 | 1 |
| EES-Lynx 2 | 08 ^h 48 ^m 43 ^s .60 | +44°53′43″ | 20.0 | 2.9 | 4.7 | >6.2 | 1 |
| EES-Lynx 3 | 08 ^h 48 ^m 42 ^s .81 | +44°54′34″ | 19.8 | 2.9 | 5.4 | >6.3 | 1 |
| EES-Lynx 4 | 08 ^h 48 ^m 48 ^s .93 | +44°57′09″ | 18.9 | 2.4 | 5.4 | 6.5 | 1 |
| SA57 1 | 13 ^h 09 ^m 15 ^s .96 | +29°16′50″ | 18.8 | 2.1 | 5.5 | 6.4 | 1 |
| SA57 2 | 13 ^h 09 ^m 19 ^s .21 | +29°20′20″ | 19.4 | 2.5 | 5.3 | 6.3 | 1 |
| SA57 3 | 13 ^h 09 ^m 19 ^s .80 | +29°21′05″ | 18.9 | 2.2 | 5.1 | 6.7 | 1 |
| EES-Pisces 1 | 23 ^h 12 ^m 52 ^s .93 | +00°57′06″ | 19.8 | 3.5 | 6.0 | >7.4 | 1 |
| EES-Pisces 2 | 23 ^h 12 ^m 48 ^s .31 | +01°00′09″ | 20.1 | 1.7 | 6.7 | >6.6 | 1 |
| EES-Cetus 1 | 03 ^h 01 ^m 26 ^s .85 | +00°21′50″ | 19.9 | 2.3 | 5.1 | 6.5 | 1 |
| EES-Cetus 2 | 03 ^h 01 ^m 41 ^s .46 | +00°22′32″ | 20.0 | 2.8 | 5.6 | 5.5 | 1 |
| EES-Cetus 3 | 03 ^h 01 ^m 24 ^s .74 | +00°22′31″ | 20.2 | 2.3 | 5.8 | >6.0 | 1 |
| EES-Cetus 4 | 03 ^h 01 ^m 25 ^s .44 | +00°23′18″ | 20.1 | 2.4 | >6.4 | >6.0 | 1 |
| EES-Cetus 5 | 03 ^h 01 ^m 24 ^s .97 | +00°25′28″ | 20.0 | 2.2 | 5.4 | 6.2 | 1 |
| Other EROs from literature | | | | | | | |
| ERO-1 | 13 ^h 12 ^m 14 ^s .04 | +42°43′55″ | 19.3 | ... | 6.2 | ... | 2 |
| ERO-2 | 16 ^h 44 ^m 57 ^s .08 | +46°26′03″ | 18.7 | 2.7 | 6.2 | ... | 3 |
| ERO-3 | 17 ^h 21 ^m 46 ^s .14 | +50°02′51″ | 19.6 | ... | 6.4 | 8.4 | 8 |
| ERO-5 | 21 ^h 07 ^m 15 ^s .29 | +23°31′20″ | 19.7 | ... | >6.6 | ... | 4 |
| ERO-6 | 21 ^h 07 ^m 15 ^s .46 | +23°31′38″ | 19.8 | ... | >6.5 | ... | 4 |
| ERO-7 | 22 ^h 17 ^m 33 ^s .24 | +00°16′04″ | 19.6 | ... | >6.0 | ... | 5 |
| ERO-8 | 22 ^h 17 ^m 33 ^s .24 | +00°14′28″ | 20.3 | ... | >6.0 | ... | 5 |
| J0905+3408 | 09 ^h 05 ^m 30 ^s .54 | +34°08′09″ | 18.3 | ... | ... | 6.1 | 6 |
| J1046-0016 | 10 ^h 46 ^m 05 ^s .90 | -00°16′46″ | 19.4 | ... | 5.1 | ... | 7 |
| J1721+5002 | 17 ^h 21 ^m 44 ^s .50 | +50°02′06″ | 20.0 | ... | 6.2 | 6.3 | 8 |
| J1019+0534 | 10 ^h 19 ^m 31 ^s .87 | +05°34′36″ | 18.3 | ... | ... | >7.0 | 9 |
| J1205-0743 | 12 ^h 05 ^m 20 ^s .93 | -07°43′51″ | 19.2 | 2.2 | 4.7 | 5.6 | 10 |
| J1249+3350 | 12 ^h 49 ^m 43 ^s .17 | +33°50′04″ | 19.7 | ... | >4.9 | >6.3 | 11 |

^a Though the sample was chosen with $K < 20$, a revision of the photometry after sample selection resulted in a few objects with $K > 20$.

1: Elston, R. et al. 2001, in preparation; 2: Cowie, L. L. et al. 1996, AJ, 112, 839; 3: Hu, E. M. & Ridgway, S. E. 1994, AJ, 107, 1303; 4: Knopp, G. P. & Chambers, K. C. 1997, ApJS, 109, 367; 5: Cowie, L. L. et al. 1994, ApJ, 434, 114; 6: Eisenhardt, P. & Dickinson, M. 1992, ApJ, 399, L47 ; 7: Moustakas, L. A. et al. 1997, ApJ, 475, 445; 8: McLeod, B. A. et al. 1995, ApJS, 96, 117; 9: Dey, A. et al. 1995, ApJ, 440, 515; 10: Giallongo, E. private communication; 11: Soifer, B. T. et al. 1994, ApJ, 420, L1

array provides 0.6'' pixels over a $\sim 2.5'$ field. Details of the observations and data analysis are given in Elston et al. (2001). The *BRIzJK* survey images were co-aligned and convolved to the same effective PSF of $FWHM \sim 1.5''$. Calibrations of the optical and IR images onto the Landolt and CIT systems were obtained using observations of Landolt and UKIRT standard stars, respectively.

A catalogue of objects within each of the four fields of the EES survey was obtained from the K images using SExtractor (Bertin & Arnout 1996). Object detection was performed down to a level corresponding to 1.5σ above the sky level, with a minimum object size of 1.2 square arc-seconds. Photometry was obtained through 3.3'' diameter apertures using this catalog on the *BRIzJK* images; the 4σ limit in the K band is 21.4. Details of these catalogues are available in Elston et al. (2001).

2.2. SCUBA observations at the JCMT

A sub-sample was observed with Submillimeter Common-User Bolometer Array (SCUBA) instrument on the James Clerk Maxwell Telescope (JCMT) at 450 μm and 850 μm in the standard point-source photometry mode during different observing runs from 1998 to 2000. The typical opacity τ was in the range 0.2–0.5 and 2–4 at 850 μm and 450 μm respectively. The on-source integration times varied between 900 and 3600 s. The data reduction was performed using the Starlink SURF software (Jenness & Lightfoot 1998). For each integration, the measurements in the reference beam were subtracted from those in the signal beam, rejecting obvious spikes. Flat-field corrections were applied to each observation which were subsequently corrected for atmospheric opacity. The residual sky background emission was then removed using the

median of the outputs of the different rings of the bolometer as a background estimate. The flux calibration of the data was performed mainly using a primary calibrator (Uranus or Mars), thus yielding a 10% accuracy for the flux density scale. A poorer calibration accuracy (20%) was obtained for EES Lynx 2 and SA57 2–3 for which the secondary calibrators CRL618 and HL Tau were used respectively. The individual reduced and calibrated observations were concatenated for each source thus obtaining a final co-added data set.

2.3. IRAM 30 m telescope observations

The 1.25 mm data reported here were taken with the MPIFR 37-channel and 19-channel bolometers (Kreysa et al. 1998) at the focus of the IRAM 30 m antenna (Pico Veleta, Spain) during observing runs in March 1998 and December 1998 respectively. The filter set used combined with atmospheric transmission produces an effective wavelength of about 1.25 mm; the beam size is $11''$ (*FWHM*) and the chop throw was set at $50''$ and $30''$, during the first and second run, respectively. The expected average sensitivity for each channel, limited principally by atmospheric noise, was $60 \text{ mJy}/\sqrt{BW}$, where BW is the bandwidth used, in Hz. However, the 37-channel bolometer observations were noisier than expected and therefore the 19-channel bolometer was used for the second observing run. The effect of sky noise was reduced substantially by exploiting the correlation between signals from the different channels using the standard three beam (beam-switching + nodding) technique, resulting in an average rms 1σ value, after 6000 s of integration, of 0.57 mJy and 0.4 mJy for the 37-channel and 19-channel data respectively. The typical on-source integration time was 6000 s, distributed over two to three nights. The atmospheric transmission was monitored by making frequent sky-dips. The average zenith opacity was 0.13 during the observations in March, with a maximum of 0.2, and the average opacity was ~ 0.3 during the December observing run. Absolute flux calibration was performed using Uranus as the primary calibrator and using Mars and quasars from the IRAM pointing list as secondary calibrators. The different calibration measurements were consistent at a level of 5% for both planets. Including the uncertainty in the planet temperatures, the average flux calibration uncertainty was estimated to be 10%. Pointing was checked every hour and the average accuracy achieved was better than $3''$.

The data were reduced assuming that the target sources are unresolved, i.e. the source sizes at mm wavelengths are smaller than the size of the central channel. The remaining 36 and 18 channels (excluding one which suffered a large electronic loss) were then used to derive a low-noise sky estimate. The average value of the sky brightness, computed using these outer 35 and 17 channels respectively, was subtracted from the signal in the central channel to derive the final flux density estimates.

2.4. VLA observations

The Very Large Array (VLA) was used to observe a total of 16 EROs distributed in six different fields.

4.8 GHz radio continuum emission was searched for in eleven of these objects in the D configuration at 4.8 GHz, chosen as a compromise between optimising point source sensitivity using a low resolution array and minimizing confusion through the usage of a high resolution array. The correlator was used in the continuum mode and data were acquired in 4 IF bands, each of 50 MHz bandwidth.

The flux calibration and initial phase calibration was done using standard techniques described in Taylor et al. (1999) and the data reduction was done using standard algorithms in the software AIPS. Self-calibration of only the visibility phases was done for a few fields using background sources in the primary beam. The rms noise in the final images is within 20% of the expected thermal noise.

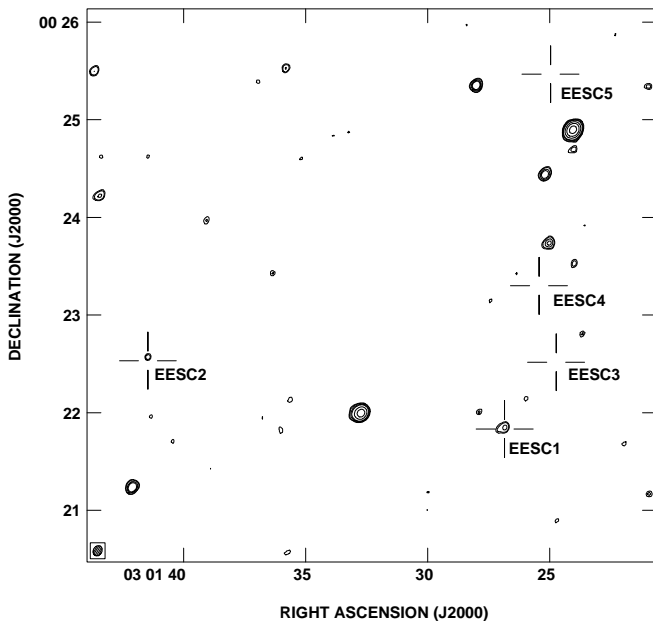
Seven EROs distributed in two fields were observed using the VLA in the B configuration at 1.4 GHz. The frequency of observation was chosen based on the expected steep spectral index of the continuum emission of EROs (typically -0.7) and poor sensitivity of the VLA at $\nu < 1$ GHz. Optimising between confusion and the slightly extended nature of EROs ($\geq 2''$) led to the B configuration being used (the number of sources within a synthesised beam area in this configuration with flux densities higher than 1σ for 8 hours of integration is 0.015, using the relation given in Langston et al. 1990). These observations were made in the line mode using 4 IFs, each with a bandwidth of 25 MHz and 7 available channels (the 50 MHz bandwidth system was not used at this frequency as much higher closure errors are expected: Owen, private communication). The dataset were hanning smoothed following standard calibration procedures and were imaged using multi-band synthesis (in order to reduce the effect of bandwidth smearing far from the phase centre). The tangent-plane approximation was used to correct for the effects of the array non-coplanarity and strong sources within two primary beams of the phase centre were isolated by defining multiple fields and simultaneously deconvolved using the CLEAN algorithm. Self-calibration using sources in the primary beam was done only for the visibility phases and the data were flagged based on excessive closure errors. An rms within 20% of the theoretical noise was achieved for the EES-Pisces field but the noise in the EES-Cetus field was substantially higher due to the presence of strong sources near the phase centre. Further details are given in Table 2.

3. Results

Out of the seven sources observed at $1250 \mu\text{m}$, one source, SA57-1, was marginally detected at the 3σ level. The measured flux densities at the NIR positions of the EROs along with the 1σ errors are listed in Table 3 for the $450 \mu\text{m}$, $850 \mu\text{m}$ and the $1250 \mu\text{m}$ data. As can be seen, none of

Table 2. Log of VLA observations.

| Field | # of EROs | Phase Calibrator | Date of Obs. | rms (μ Jy) | CLEAN beam |
|----------------------------------|-----------|------------------|--------------|-----------------|----------------------|
| 4.8 GHz VLA D Array Observations | | | | | |
| ERO-1 | 1 | 1327+434 | 28 May 1999 | 18 | $34'' \times 17''$ |
| ERO-5 | 1 | 2115+295 | 28 May 1999 | 15 | $20'' \times 17''$ |
| EES-Lynx | 4 | 0818+423 | 28 May 1999 | 14 | $19'' \times 16''$ |
| SA57 | 3 | 1310+323 | 29 May 1999 | 14 | $27'' \times 15''$ |
| EES-Pisces | 2 | 2323-032 | 28 May 1999 | 16 | $25'' \times 16''$ |
| 1.4 GHz VLA B Array Observations | | | | | |
| EES-Pisces | 2 | 2323-032 | 12 Nov. 1999 | 18 | $7'' \times 5''$ |
| EES-Cetus | 5 | 0323+055 | 6 Nov. 1999 | 75 | $6.5'' \times 5.3''$ |

**Fig. 1.** Contour plot of the 1.4 GHz continuum image of the EES-Cetus field. The centres of the stars mark the NIR positions of the EROs. The two detections, EESC1 and EESC2 can be seen. The CLEAN beam is $6.5'' \times 5.3''$ and is shown in the bottom left corner of the figure. The rms is 75μ Jy. The contour levels are at 3.3σ , 4σ , 6σ , 8σ , 17σ , 32σ & 63σ .

the other observed sources were detected at these wavelengths.

We have detected 1.4 GHz radio continuum emission from the NIR positions of two EROs: EES-Cetus 1 and EES-Cetus 2 (hereafter, EESC1 and EESC2). None of the other sources observed at either 4.8 GHz or 1.4 GHz were detected and the corresponding measurements at the expected NIR positions and the 1σ errors are given in Table 3. The 1.4 GHz image of the EES-Cetus field with the two detections is shown in Fig. 1. Though there appears to be some extended emission in the image of EESC1, given the signal-to-noise ratios of the two detections, the two sources are essentially unresolved. We estimate the likelihood of these two radio sources being the counterparts of the NIR-detected EROs as follows: the positional error in the radio positions is calculated for the two sources using the relations given in Rieu (1969).

We assume the error in the NIR position to be $0.5''$, which is the 1σ error between the radio and the optical reference frames (Russell et al. 1990). The value of the likelihood ratio (LR) as defined by de Ruiter et al. (1977) is calculated to be 1276 for EESC1 and 43 for EESC2, using the relation in Langston et al. (1990) to estimate the surface density of objects with $S_{1.4 \text{ GHz}} > 0.1 \text{ mJy}$.

This implies that the a posteriori probabilities of the radio detections being actual counterparts are 99.92% and 97.73% for EESC1 and EESC2 respectively (assuming that the a priori probability that the ERO does have a radio counterpart is 50%). Hence the radio counterpart to EESC1 seems real but the identification of the counterpart of EESC2 is slightly less secure.

4. Statistical properties of the sample

Though almost the entire sample is undetected at all observed wavelengths, the flux densities measured at the IR positions of the sources can be used to compute the statistical flux densities of the sample and hence derive stricter upper limits. This weighted average flux density at 4.8 GHz is $3.3 \pm 4.6 \mu$ Jy for a sample of 10 objects observed (the value for the 1.4 GHz data is $-15 \pm 12 \mu$ Jy, and is far less significant in terms of the implied limits on the star formation rate). The statistical flux density at $850 \mu\text{m}$ for the entire sample of 21 EROs is $1.0 \pm 0.4 \text{ mJy}$ and the corresponding number for the $1250 \mu\text{m}$ measurements is $0.18 \pm 0.12 \text{ mJy}$ for 15 sources. Clearly, the $1250 \mu\text{m}$ and the 4.8 GHz data do not yield a statistical detection of the ERO population whereas the $850 \mu\text{m}$ data yields a marginal 2.5σ statistical detection. A similar exercise was carried out for the EES sample as well and the average flux densities at 4.8 GHz, $1250 \mu\text{m}$ and $850 \mu\text{m}$ are $3.5 \pm 4.8 \mu$ Jy, $0.18 \pm 0.13 \text{ mJy}$ and $0.3 \pm 0.6 \text{ mJy}$ for nine, seven and fourteen objects respectively; there is no statistical detection for this complete sample either. We have quoted the values for the 4.8 GHz and the $1250 \mu\text{m}$ data for the EES sample though not all sources have been observed, as the observed sources probably form a random sub-sample of the complete sample since they were selected based on telescope scheduling constraints. The 2.5σ result for the average $850 \mu\text{m}$ flux density for the entire sample can be traced solely to the non-EES

Table 3. Radio, mm and sub-mm flux densities of EROs.

| Galaxy | 1250 μm (mJy) | error (mJy) | 850 μm (mJy) | error (mJy) | 450 μm (mJy) | error (mJy) | 4.8 GHz (μJy) | error (μJy) | 1.4 GHz (μJy) | error (μJy) |
|-----------------------------------|-----------------------------|----------------|----------------------------|----------------|----------------------------|----------------|-------------------------------|-----------------------------|-------------------------------|-----------------------------|
| EES Sample | | | | | | | | | | |
| EES-Lynx 1 | ... | ... | -1.6 | 1.8 | ... | ... | 19.0 | 14.0 | ... | ... |
| EES-Lynx 2 | ... | ... | -0.1 | 2.0 | ... | ... | 10.6 | 14.0 | ... | ... |
| EES-Lynx 3 | ... | ... | 1.2 | 1.7 | ... | ... | 5.4 | 14.0 | ... | ... |
| EES-Lynx 4 | -0.1 | 0.3 | -0.8 | 2.6 | ... | ... | -4.9 | 14.0 | ... | ... |
| SA57 1 | 1.5^a | 0.5 | 2.9 | 1.6 | ... | ... | -12.0 | 14.0 | ... | ... |
| SA57 2 | 0.8 | 0.4 | 3.5 | 2.3 | ... | ... | -5.0 | 14.0 | ... | ... |
| SA57 3 | -0.3 | 0.4 | -5.6 | 2.7 | ... | ... | 16.0 | 14.0 | ... | ... |
| EES-Pisces 1 | ... | ... | -1.9 | 1.9 | ... | ... | 2.6 | 16.0 | -11.0 | 18.0 |
| EES-Pisces 2 | -0.3 | 0.2 | -1.0 | 1.9 | ... | ... | -1.5 | 16.0 | -27.0 | 18.0 |
| EES-Cetus 1 | ... | ... | 0.7 | 2.4 | 11 | 45 | ... | ... | 520.0^a | 75.0 |
| EES-Cetus 2 | 0.2 | 0.4 | 2.4 | 2.8 | 128 | 118 | ... | ... | 380.0^a | 75.0 |
| EES-Cetus 3 | ... | ... | -0.9 | 2.1 | 5 | 29 | ... | ... | -14.0 | 75.0 |
| EES-Cetus 4 | 0.5 | 0.4 | 1.9 | 2.1 | 17 | 23 | ... | ... | 70.0 | 75.0 |
| EES-Cetus 5 | ... | ... | 1.8 | 2.3 | 33 | 32 | ... | ... | 47.0 | 75.0 |
| Other EROs from literature | | | | | | | | | | |
| ERO-1 | 0.7 | 1.4 | 1.7 | 1.1 | ... | ... | 0.4 | 18.0 | <14 ^b | ... |
| ERO-2 | -0.8 | 1.3 | 1.1 | 4.7 | ... | ... | ... | ... | ... | ... |
| ERO-3 | 0.1 | 1.1 | -0.9 | 3.9 | ... | ... | ... | ... | ... | ... |
| ERO-5 | ... | ... | 2.2 | 1.1 | ... | ... | <70 ^c | ... | ... | ... |
| ERO-6 | ... | ... | 3.1 | 2.9 | ... | ... | ... | ... | ... | ... |
| ERO-7 | ... | ... | 4.2 | 2.2 | ... | ... | ... | ... | ... | ... |
| ERO-8 | ... | ... | -0.5 | 2.1 | ... | ... | ... | ... | ... | ... |
| J0905+3408 | 0.1 | 0.9 | ... | ... | ... | ... | ... | ... | ... | ... |
| J1046-0016 | 0.4 | 1.7 | ... | ... | ... | ... | ... | ... | ... | ... |
| J1721+5002 | 0.4 | 1.1 | ... | ... | ... | ... | ... | ... | ... | ... |
| J1019+0534 | -1.6 | 1.7 | ... | ... | ... | ... | ... | ... | ... | ... |
| J1205-0743 | -0.7 | 1.7 | ... | ... | ... | ... | ... | ... | ... | ... |
| J1249+3350 | -0.7 | 1.3 | ... | ... | ... | ... | ... | ... | ... | ... |

^a The three entries in bold face are detections. The rest are the flux densities measured at the NIR positions of the EROs, with the associated 1σ error. These values have been used to calculate the statistical flux densities of the sample (see Sect. 4).

^b 3σ upper limit: Richards, private communication.

^c The upper limit to the 4.8 GHz flux density of ERO-5 is quoted as this source is 1.5 synthesized beams away from a strong confusing source.

sample of 7 galaxies, whose mean signal to noise ratio is 1σ . Therefore it is probable that some of these EROs not in the EES sample might be detectable at 850 μm if observed further. In this paper, we will take the 3σ upper limit of 1.2 mJy for the average flux density at this wavelength for the entire ERO sample.

The sample was also divided into two sub-samples using an $I - K$ colour cut-off (various cut-off values ranging from 5.3 to 5.9 were tried) and it was seen that there is no statistically significant difference in the average flux densities between the two sub-samples. This result holds for the EES sample as well.

If the observed population is divided into ellipticals and starbursts using the $I - K$ versus $J - K$ diagram of

Pozzetti & Mannucci (2000), described in Sect. 5.1, the two categories of EROs do not differ in their average flux densities either, within errors.

5. Ellipticals or starbursts?

Though attempts to distinguish between pure starbursts and elliptical galaxies among the ERO population have met with unambiguous results only for sources bright in IR and optical, or for sources with detectable mm/sub-mm emission, a few recent studies seem to show that probably $\geq 70\%$ of the EROs are old high redshift ellipticals. The evidence for this is based on both individual spectroscopic identifications of small samples of EROs

(Cimatti et al. 1999; Liu et al. 2000) and on high resolution images, using morphological information (Stiavelli & Treu 2001) and through fitting the de Vaucouleurs' law to radial profiles (Moriondo et al. 2000). Additionally, a recent wide-field survey of EROs by Daddi et al. (2000a) has shown that these objects are strongly clustered in the sky and this result has been confirmed in two other fields by McCarthy et al. (2000). The strong clustering of the ERO population is added evidence that the majority of EROs are indeed ellipticals, since ellipticals are known to be more clustered than spirals, and also because of the narrow range of redshift, $z = 1-2.5$, allowed for extremely red ellipticals (Daddi et al. 2000b).

5.1. Diagnostic techniques

In this section, the inferences that can be drawn from the observed multi-frequency flux densities of the EROs using group properties of ellipticals and starbursts are investigated.

It is known that the K magnitudes of radio-loud galaxies are correlated with their redshifts (Lilly & Longair 1984). It is also established that galaxies of other types have fainter K magnitudes than radio-loud galaxies at that redshift (van Breugel et al. 1999; de Breuck 2000), which can be used to set upper limits on the redshift of EROs. Given the faintness of EROs in the K band, such an exercise constrains them to lie at $z < 5$.

If we consider the upper limit to the 1.4 GHz flux density of the undetected ERO sample to be 0.1 mJy, (extrapolated from the 4.8 GHz upper limit. This excludes the EROs observed at 1.4 GHz which have varying upper limits and excludes the two detections as well) then for $z < 5$, the rest frame 1.4 GHz luminosity is less than 2×10^{25} W/Hz for $\Omega_\Lambda = 0.7$ (and less than 6×10^{24} W/Hz for $\Omega_\Lambda = 0$). From the bi-modal 1.4 GHz luminosity distribution of the IRAS 2 Jy sample (Fig. 15 of Yun et al. 2001), it is clear that our sample cannot be differentiated into galaxies dominated by starbursts versus those by AGNs, which reflects the fact that our radio data is not deep enough to detect weak starbursts.

Pozzetti & Mannucci (2000) showed that old ellipticals and dusty starbursts occupy distinctly different areas in the $I - K$ versus $J - K$ diagram and derived the theoretical dividing line in this plane. Due to the faintness of most EROs in the K band, the error bars for the colours are too large for this diagnostic to be used profitably. Additionally, HR 10, the definitive example of a dusty starburst ERO (Andreani et al. 2000; Dey et al. 1999; Cimatti et al. 1998a), lies on the dividing line. Hence, more sensitive NIR photometry is needed in order to use this method of classification.

For our sample, based on the few IR-optical colours available, and the upper limits from the radio, mm and sub-mm observations, it is not possible to determine the nature of each of the EROs individually. Instead, we now discuss the statistical properties of EROs, for the dusty

starburst galaxy and the old elliptical galaxy components, separately.

5.2. Star formation properties of EROs

The average 850 μm flux density limit can be used to derive upper bounds on the average star formation properties of the sample. Assuming that all EROs in the sample are at a redshift of 1.5 (i.e., roughly at the redshift of HR 10), we derive the average star formation rate to be less than $150 M_\odot \text{ yr}^{-1}$ (from the relation given in Carilli & Yun 1999, and assuming the dust emissivity $\beta = 1.5$) and the average FIR luminosity to be less than $1.6 \times 10^{12} L_\odot$ ($\Omega_\Lambda = 0$). For a dust temperature of 20 K, the corresponding upper limit on the average dust mass is $6 \times 10^8 M_\odot$ and for 50 K, the dust mass is less than $1.4 \times 10^8 M_\odot$. For $\Omega_\Lambda = 0.7$, $\text{SFR} < 380 M_\odot \text{ yr}^{-1}$, $L_{\text{FIR}} < 4 \times 10^{12} L_\odot$ and $M_{\text{dust}} < 2 \times 10^9 M_\odot$ for $T_{\text{dust}} = 20$ K and $< 3.6 \times 10^8 M_\odot$ for $T_{\text{dust}} = 50$ K (for a dust emissivity $\beta = 1.5$ and mass absorption coefficient of $0.15 \text{ m}^2 \text{ kg}^{-1}$ at 800 μm ; Hughes et al. 1997).

However, we can assume that a fraction x of the EROs are dusty ULIGs which resemble HR 10 in their properties ($L_{\text{FIR}} \sim 4 \times 10^{12} L_\odot$ at $z \sim 1.5$) and the rest are ellipticals with no sub-mm and mm emission. Then, from the estimated 5σ average flux densities of the ERO sample at 850 μm and 1250 μm and the measured flux densities of HR 10 ($S_{850 \mu\text{m}} = 5.5 \pm 0.6$ mJy, the weighted average of the values quoted in Cimatti et al. 1998a and Dey et al. 1999 and $S_{1250 \mu\text{m}} = 4.9 \pm 0.7$ mJy, Cimatti et al. 1998a), the value of x can be computed. Such an exercise gives $x < (36 \pm 11)\%$ and $x < (12 \pm 4)\%$ for the 850 μm and 1250 μm data respectively. This estimate, though approximate, is consistent with other independent estimates of the ULIG fraction in EROs: $\leq 30\%$ (Cimatti et al. 1999; Moriondo et al. 2000).

If we assume, as a conservative estimate, that the starburst fraction in the ERO population is as much as 30%, then from the surface density of EROs with $R - K_s \geq 5$ and $K_s \leq 19.2$ estimated by Daddi et al. (2000a), the surface density of starbursts would be less than 725 ± 33 objects deg^{-2} . Smail et al. (1999a) calculated that the surface density of SCUBA sources with a 850 μm flux density greater than 0.5 mJy (which corresponds to the cut-off estimated in order to fully explain the Far Infrared Background or FIRB) is 17000 objects deg^{-2} (for $S_{850 \mu\text{m}} \geq 2$ mJy which would explain half the observed FIRB, the surface density is 3700 objects deg^{-2}). Hence the maximum overlap between $R - K_s \geq 5$ and $K \geq 19.2$ EROs which are starbursts, and the high redshift star forming SCUBA sources is 4% (for a 0.5 mJy cut-off for $S_{850 \mu\text{m}}$; it is less than 20% for a 2 mJy cut-off).

Given the lack of detectable sub-mm emission from the sample of objects, and the estimate of the corresponding fraction of HR 10-like ULIGs, the present study clearly shows that the ULIGs like HR 10 are rather unique objects

among EROs and hence dusty strong starbursts are not the dominant component of this population.

5.3. EROs as elliptical galaxies

It can be seen from the upper limits to the radio luminosities of the EROs (derived in Sect. 5.1) that there are no radio-loud ellipticals in the sample. Hence these EROs must either be centre-brightened radio galaxies (or FR I; see Fanaroff & Riley 1974 and Ledlow & Owen 1996 for definitions). The optical luminosities have been derived assuming a median redshift of 1.5 and m_R derived from Table 1) or radio-quiet ellipticals. There are two detections at 1.4 GHz, and the 4.8 GHz upper limits of 11 EROs scaled to 1.4 GHz are ~ 0.1 mJy. Assuming that $\geq 70\%$ of these 13 EROs are elliptical galaxies, the detection rate of ellipticals for a 0.1 mJy cut-off at 1.4 GHz is calculated to be $\leq 22 \pm 16\%$. If the three EES-Cetus sources undetected in the radio are also included, the detection rate becomes $\leq 27 \pm 19\%$. For a redshift range of 1–3, 0.1 mJy at 1.4 GHz corresponds to a 1.4 GHz rest-frame radio luminosity of 2×10^{23} – 2×10^{24} W/Hz ($\Omega_\Lambda = 0$). Also, the rest-frame R band magnitude for the sample is between -18 and -25.5 (assuming a K -correction $K(z) = 1.122z$ for elliptical galaxies, see Ledlow & Owen 1996). It should be noted that for the same set of parameters, using the data published in Gavazzi & Boselli (1999), Ho (1999), Ledlow & Owen (1996) and Auriemma et al. (1977), we derive the detection rate to be 1% to $< 3\%$ for low redshift ellipticals.

6. Continuum detections – EESC1, EESC2 and SA 57-1

The two EROs, EESC1 and EESC2, with 1.4 GHz continuum detections (though the radio identification is tentative for EESC2) have only upper limits to their sub-mm flux densities. The optical-IR SED of these objects cannot be used to classify them as either elliptical or starforming galaxies unambiguously. Further, the upper limit to the $850 \mu\text{m}$ –1.4 GHz spectral index $\alpha_{1.4}^{850}$ is $+0.47$ and $+0.56$ for EESC1 and EESC2 respectively.

The ratio of radio to sub-mm flux density of a pure starburst decreases with increasing redshift, i.e., for a given sub-mm flux density, the $z = 0$ galaxies have the maximum radio flux density. Hence for a given upper limit to the sub-mm flux density for a galaxy at an arbitrary redshift, the $z = 0$ radio-FIR correlation will yield the maximum possible radio flux density. Therefore a sufficiently radio-bright AGN might possibly have a radio continuum strength higher than this value and will be easily classified as a radio-loud AGN. Since that is not so for either of the two radio detections, they cannot be unambiguously classified as either an old elliptical or a dusty starburst.

The properties of these galaxies are derived below assuming either of the two possibilities – that they are pure starbursts, or they are old ellipticals.

6.1. EESC1 and EESC2: 1.4 GHz detection

If EESC1 and EESC2 are assumed to be dominated by star formation, then from the derived upper limits to the spectral index $\alpha_{1.4}^{850}$ for EESC1 and EESC2, we can derive the upper limits to the redshifts of these objects. Carilli & Yun (2000) have tabulated the values of redshift for a given value of the spectral index $\alpha_{1.4}^{850}$ and have also tabulated the values for the $\pm 1\sigma$ curves of redshift versus $\alpha_{1.4}^{850}$. Using the derived value of $\alpha + \Delta\alpha$, where $\Delta\alpha$ is the 1σ error on the value of the spectral index α , and the z^- curve of Carilli & Yun (2000), updated in Carilli (private communication)¹, we estimate the upper limits to the redshifts (see Carilli & Yun 2000 for details).

The limiting redshifts of EESC1 and EESC2, derived as described above, are $z < 1.5$ and $z < 2.0$ respectively. Their radio continuum flux densities, if attributed solely to star formation, imply a star formation rate of about $1100 M_\odot \text{ yr}^{-1}$ and $1600 M_\odot \text{ yr}^{-1}$ respectively for the maximum redshifts derived above (these are for $\Omega_\Lambda = 0.7$). The values are about $700 M_\odot \text{ yr}^{-1}$ and $1000 M_\odot \text{ yr}^{-1}$ respectively, for $\Omega_\Lambda = 0$, and less than this value for lower values of redshift (from the relation given in Carilli & Yun 1999). Also, from the observed radio flux density, the FIR luminosity is calculated to be less than $\sim 10^{13} L_\odot$, for $z < z_{\text{max}}$, for the two galaxies.

If the two galaxies are assumed to be old ellipticals instead, then using the pure luminosity evolution models, the extreme $R - K$ colours of the two galaxies ($R - K > 6.1$) imply that they lie at redshifts greater than 1.3 (Daddi et al. 2000b). For z between 1.3 and 5, the 1.4 GHz rest-frame luminosities of EESC1 and EESC2 correspond to the luminosity range of FR I galaxies or radio-quiet ellipticals.

6.2. SA57-1: 1.25 mm IRAM detection?

SA57-1 is detected at 1.25 mm with the IRAM 30 m telescope at the 3σ level: $S_{1.25 \text{ mm}} = 1.45 \pm 0.45$ mJy. Assuming that this detection is real, it is not obvious whether this source is a pure starburst or whether it also harbours an AGN. From the 1.25 mm measurement and the upper limit to the radio emission, a lower limit of 0.9 can be derived for the redshift of the object (using the z^+ curve in Carilli & Yun 2000), as described in Sect. 5.1. This is also the lower limit to z if SA57-1 is an elliptical galaxy. Using the $K - z$ relation for radio-loud galaxies, the derived upper limit to the redshift is 3.5. If this object were a pure starburst, the implied SFR is between 45 – $800 M_\odot \text{ yr}^{-1}$ for $\Omega_\Lambda = 0$ (and 70 – $1300 M_\odot \text{ yr}^{-1}$ for $\Omega_\Lambda = 0.7$). The corresponding L_{FIR} is greater than $4.5 \times 10^{10} L_\odot$.

¹ The updated values can be found at the URL: <http://www.aoc.nrao.edu/~ccarilli/alphaz.shtml>.

7. Conclusions

Motivated by the discovery of HR 10 and its star formation properties, a sample of EROs was observed in order to detect radio, mm and sub-mm continuum emission and constrain the redshifts and star formation rates of ULIGs in the sample. One ERO was detected at 1.4 GHz and a possible radio counterpart was identified for another ERO at the same frequency. A third was tentatively identified at 1250 μm . Their redshifts and star forming properties were constrained using their radio-FIR spectral index but their nature could not be unambiguously determined. Since the sources are faint, standard techniques to classify the sources in the ERO sample individually as ellipticals or starburst are inadequate. Weighted average flux densities were computed for the sample using measurements at the IR positions of the EROs and these values are 1.0 ± 0.4 mJy at 850 μm , 0.18 ± 0.12 mJy at 1250 μm and 3.3 ± 4.6 μJy at 4.8 GHz. We find no difference within errors in the weighted average values between EROs with NIR colours above and below an assumed $I - K$ colour cut-off. If the sample is divided into ellipticals and starbursts based on the NIR two-colour diagnostic diagram, no differences in their average flux densities are seen between these groups. From the lack of detection of sub-mm emission from any of the EROs in our sample, it is now clear that dusty strong starbursts, or high redshift ULIGs, are not the dominant component of this population. If it is assumed that such an ULIG population would resemble HR 10 in their SED properties, then such galaxies cannot constitute more than about 35% of the EROs. From the observed source counts of SCUBA sources and the ERO surface density, we suggest that EROs contribute negligibly to both high redshift star formation as well as to the FIRB. On the other hand, if all EROs have similar star formation properties, the average dust mass is calculated to be less than $2 \times 10^9 M_{\odot}$ (for $\Omega_{\Lambda} = 0.7$ and $T_{\text{dust}} = 20$ K) and the average FIR luminosity, less than $4 \times 10^{12} L_{\odot}$. If not more than a third of the EROs in the sample are assumed to be starbursts and the rest are assumed to be ellipticals at a median redshift of 1.5, we calculate the detection rate of ellipticals for a 0.1 mJy cut-off at 1.4 GHz to be less than $22 \pm 16\%$. The corresponding number estimated in the local universe is $\leq 3\%$.

Therefore it is clear that the dominant population of EROs are not ULIGs similar to HR 10 but are probably old ellipticals and weaker starbursts. The determination of the properties and redshifts of the elliptical galaxy component of the ERO population is extremely important for constraining structure formation models (Daddi et al. 2000b). Towards this end, the upper limits to the radio and the sub-mm flux densities derived in this study should be used to plan future observations to detect these objects at these wavebands.

Acknowledgements. The JCMT is operated by the Joint Astronomy Centre, on behalf of the UK Particle Physics and Astronomy Research Council, The Netherlands Organization for Scientific Research (NWO) and the Canadian research

council. The VLA is a facility of the National Radio Astronomy Observatory (NRAO), which is operated by Associated Universities, Inc. under a cooperative agreement with the National Science Foundation. This work was based on observations carried out with the IRAM 30 m telescope. IRAM is supported by INSU/CNRS (France), MPG (Germany) and IGN (Spain). This research has made use of NASA's Astrophysics Data System Abstract Service. We thank Wolfgang Tschager for help with the IRAM observations. Part of this work was done by NRM during his visit at Leiden Observatory and he thanks the Netherlands Research School for Astronomy (NOVA), Leids Kerkhoven-Bosscha Fonds and Leiden observatory for financial support and the staff of Leiden Observatory for their hospitality and stimulating discussions. NRM also acknowledges useful discussions with Frazer Owen and K. S. Dwarakanath about data analysis and K. R. Anantharamaiah for encouragement in moving on to higher redshift realms.

References

- Andreani, P., Cimatti, A., Röttgering, H. J. A., & Tilanus, R. 1999, *Ap&SS*, 266, 267
- Andreani, P., Cimatti, A., Loinard, L., & Röttgering, H. 2000, *A&A*, 354, L1
- Auremma, C., Perola, G. C., Ekers, R., et al. 1977, *A&A*, 57, 41
- Bertin, E., & Arnouts, S. 1996, *A&AS*, 117, 393
- Blain, A. W. 1999, *MNRAS*, 309, 955
- Carilli, C. L., & Yun, M. S. 1999, *ApJ*, 513, L13
- Carilli, C. L., & Yun, M. S. 2000, *ApJ*, 530, 618
- Chapman, S. C., McCarthy, P. J., & Persson, S. E. 2000, *AJ*, 120, 1612
- Cimatti, A., Andreani, P., Röttgering, H., & Tilanus, R. 1998a, *Nature*, 392, 895
- Cimatti, A., Andreani, P., Röttgering, H. J. A., & Tilanus, R. 1998b, in *Proc. of the Xth Rencontres de Blois, The Birth of Galaxies* [[astro-ph/9810004](#)]
- Cimatti, A., Daddi, E., di Serego Alighieri, S., et al. 1999, *A&A*, 352, L45
- Cimatti, A. 2000, in *Proc. of the ESO/ECF/STScI workshop, Deep Fields* [[astro-ph/0012057](#)]
- Condon, J. J. 1992, *ARA&A*, 30, 575
- Daddi, E., Cimatti, A., Pozzetti, L., et al. 2000a, *A&A*, 361, 535
- Daddi, E., Cimatti, A., & Renzini, A. 2000b, *A&A*, 362, L45
- De Ruiter, C. 2000, Ph.D. Thesis
- de Bruiter, H. R., Arp, H. C., & Willis, A. G. 1977, *A&AS*, 28, 211
- Dey, A., Graham, J. R., Ivison, R. J., et al. 1999, *ApJ*, 519, 610
- Elston, R., Rieke, G. H., & Rieke, M. J. 1988, *ApJ*, 331, L77
- Elston, R., et al. 2001, in preparation
- Fanaroff, B. L., & Riley, J. M. 1974, *MNRAS*, 167, 31
- Gavazzi, G., & Boselli, A. 1999, *A&A*, 343, 86
- Gear, W. K., et al. 2001, *MNRAS*, in press
- Graham, J. R., & Dey, A. 1996, *ApJ*, 471, 720
- Ho, L. C. 1999, *ApJ*, 510, 631
- Hu, E. M., & Ridgway, S. E. 1994, *AJ*, 107, 1303
- Hughes, D. H., Dunlop, J. S., & Rawlings, S. 1997, *MNRAS*, 289, 766
- Jenness, T., & Lightfoot, J. F. 1998, *ADASS VII*, ed. R. Albrecht, R. N. Hook, & H. A. Bushouse, *ASP Conf. Ser.*, 145, 216

- Kreysa, E., Gemuend, H.-P., Gromke, J., et al. 1998, in *Advanced Technology MMW, Radio, and Terahertz Telescopes*, ed. T. G. Phillips, Proc. of SPIE vol. 3357, 319,
- Langston, G. I., Conner, S. R., Heflin, M. B., Lehar, J., & Burke, B. F. 1990, *ApJ*, 353, 34
- Ledlow, M. J., & Owen, F. N. 1996, *AJ*, 112, 9
- Lilly, S. J., & Longair, M. S. 1984, *MNRAS*, 211, 833
- Liu, M. C., Dey, A., Graham, J. R., et al. 2000, *AJ*, 119, 2556
- McCarthy, P. J., Persson, S. E., & West, S. C. 1992, *ApJ*, 386, 52
- McCarthy, P. J., et al. 2000, in Proc. of the ESO/ECF/STScI workshop, *Deep Fields* [[astro-ph/0011499](#)]
- Moriondo, G., Cimatti, A., & Daddi, E. 2000, *A&A*, 364, 26
- Pozzetti, L., & Mannucci, F. 2000, *MNRAS*, 317, L17
- Rieu, N.-Q. 1969, *A&A*, 1, 128
- Russell, J. L., Lasker, B. M., McLean, B. J., Sturch, C. R., & Jenkner, H. 1990, *AJ*, 99, 2059
- Smail, I., Ivison, R., Blain, A., & Kneib, J.-P. 1999a, *Ap&SS*, 266, 279
- Smail, I., Ivison, R. J., Kneib, J.-P., et al. 1999b, *MNRAS*, 308, 1061
- Soifer, B. T., Matthews, K., Neugebauer, G., et al. 1999, *AJ*, 118, 2065
- Spinrad, H., Dey, A., Stern, D., et al. 1997, *ApJ*, 484, 581
- Stiavelli, M., & Treu, T. 2001, in Proc. of Galaxy Disks and Disk Galaxies, ed. J. G. Funes, & E. M. Corsini, ASP Conf. Ser. 230, 603 [[astro-ph/0010100](#)]
- Taylor, G. B., Carilli, C. L., & Perley, R. A. 1999, *Synthesis Imaging in Radio Astronomy II*, Sixth NRAO/NMIMT Synthesis Imaging Summer School, ASP Conf. Ser., 180
- Thompson, D., Beckwith, S. V. W., Fockenbrock, R., et al. 1999, *ApJ*, 523, 100
- van Breugel, W., De Breuck, C., Stanford, S. A., et al. 1999, *ApJ*, 518, L61
- Walsh, D. E. P., Knapp, G. R., Wrobel, J. M., & Kim, D. W. 1989, *ApJ*, 337, 209
- Yan, L., McCarthy, P. J., Weymann, R. J., et al. 2000, *AJ*, 120, 575
- Yun, M. S., Reddy, N. A., & Condon, J. J. 2001, *ApJ*, 554, 803